16th ICAAR LISBOA 2020-2022

16th International Conference on
Alkali-Aggregate Reaction in Concrete
Lisboa | LNEC | Portugal | 31 May - 2 June 2022

http://icaar2020-2022.lnec.pt

Meso-scale modelling of ASR in concrete: effect of viscoelasticity

Emil Gallyamov [(1)], Roozbeh Rezakhani [(2)], Mauro Corrado [(3)], Jean-François Molinari [(1)]

(1) Civil Engineering Institute, Materials Science and Engineering Institute, École Polytechnique Fédérale de Lausanne (EPFL), Lausanne, Switzerland, emil.gallyamov@epfl.ch

(2) Department of Mechanical Engineering and Material Science, Duke University, Durham, USA

(3) Department of Structural, Geotechnical and Building Engineering, Politecnico di Torino, Turin, Italy

Abstract

A meso-scale numerical model for simulating damage in concrete due to ASR is presented. It accounts for the internal structure of concrete including aggregates and mortar. ASR sites are explicitly represented. This model is extended to account for viscoelastic effects in the mortar. An ASR product expansion law is based on the phenomenological reaction extent equation. The model is calibrated on free ASR expansion experiments. Mortar is modelled both as elastic- and viscoelastic-brittle material. In case of the viscoelastic-brittle mortar, simulations result in a lower level of damage and lower stiffness reduction than in the elastic-brittle case. However, the macroscopic expansion becomes lower than the experimental values. This suggests that to reach sufficient macroscopic strain, a larger damage extent within aggregates is necessary.

***Keywords**: alkali-silica reaction; sequential linear analysis; viscoelasticity*

1. INTRODUCTION

Alkali-silica reaction (ASR) is a swelling reaction in concrete that leads to continuous degradation of its properties. This reaction takes place between the amorphous silica contained in aggregates and the alkali coming from cement paste, leading to the formation of the expansive ASR product. The internal stress exerted on concrete by this product leads to its cracking and loss of bearing capacity. Damage in concrete due to ASR depends on various factors, e.g. temperature, humidity, availability of reactants, and stress state.

With high enough amount of water and reactants, ASR causes the development of a whole network of coalesced cracks. Under isotropic loading conditions and no reinforcement, cracks have irregular patterns. Presence of a prevailing loading direction or internal steel reinforcement results in “oriented” crack network.

ASR has been investigated by both laboratory experiments and numerical simulations extensively. Since ASR has been strongly affecting such large structures as bridges and dams, most of the developed numerical models are macroscopic. They simulate concrete as a homogeneous isotropic media without considering processes happening at the micro-scale. However, in order to understand the physics behind the ASR damage, the development of micro- and meso-scale mechanical models is necessary.

Dunant and Scrivener [1] proposed a two-dimensional finite element model where the internal structure of concrete is directly represented and ASR product is randomly distributed across it. Cuba Ramos et al. [2] proposed an efficient scheme to parallelize the aforementioned model. The authors performed simulations of ASR-affected concrete and concluded that their model significantly overestimates the loss of macroscopic stiffness. As one of the possible reasons for the discrepancy between simulations and experimental data, they suggested the absence of viscous energy dissipation in the mortar. Researchers studying the tensile cracking of concrete due to early-age shrinkage report that the stress relaxation delays the onset of cracking by reducing the tensile stress significantly. Other studies report values of this reduction in the range of 20 − 60% depending on the ratio between the initial load and the ultimate capacity, as well as the age of loading [3]. Giorla et al. [4] developed the space-time finite elements formulation for generalised viscoelastic materials and used it to study the effects of viscoelasticity in ASR. However, this formulation is complicated in implementation and requires can not be simply built on top of the existing finite element code. In the current study, we propose a simple finite element model to account for viscoelasticity in brittle materials and use it to study the effect of viscoelasticity on the mechanical behavior of concrete undergoing ASR.

The outline of the paper is as follows. First, the proposed meso-scale model is described in Section 2. In Subsections 2.1 and 2.2 material behavior of aggregates and mortar are explained. The temperature-dependent ASR product expansion law is recapitulated in Subsection 2.3. In Section 4, simulation results on deformations, damage and stiffness reduction are presented in a comparative manner. Finally, conclusions are given.

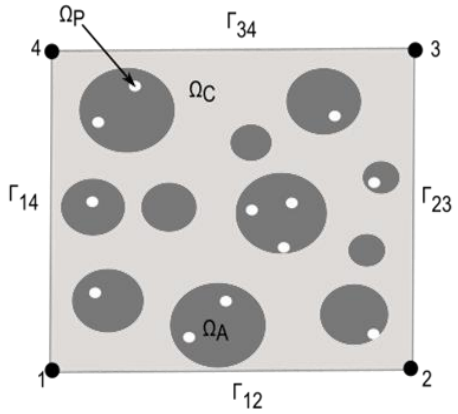

Figure 1.1: Schematic of the meso-scale model

2. MESO-SCALE MODEL

At the meso-scale, a two-dimensional domain Ω is descritized using finite elements. It represents the ASR-affected concrete laboratory specimen and contains three mutually exclusive phases: the aggregates Ω_A, the mortar Ω_C, and the ASR sites Ω_P as shown in Fig. 1.1. The isotropic eigenstrain ε_{eig} with only diagonal terms is applied at each ASR product site. The eigenstrain ε_{eig} and the elastic strain ε_{el} are connected through the following equation:

$$\varepsilon = \varepsilon_{el} + \varepsilon_{eig}\,, \tag{1}$$

where ε is the infinitesimal strain tensor. ASR sites are randomly distributed within aggregates.

Mechanics of the ASR product accounts for different phenomena taking place in a range of scales varying from nanometer to millimeter, and not yet fully understood. These processes include the growth of ASR product (either amorphous or crystalline), the opening of micro-cracks due to that, possible transport of product into pores and fissures, change of its properties with time and the surrounding environment. Leeman and colleagues [5-6] had previously shown that the primary ASR product starts to accumulate between mineral grains within reactive concrete aggregates. Therefore a typical size of an ASR inclusion is few nanometers. In the current numerical study, the average size of a finite element 0.5 millimeters. Therefore, the expansion that we apply at a single finite element to represent the effect of ASR, should be seen as a homogenized expansion of an aggregate surrounding a single pocket of the ASR product, rather than the expansion of product itself. The law describing the increase of the eigenstrain will be discussed further.

Since the concrete damage due to ASR is an extremely slow process, quasi-static conditions are assumed. The equation for the virtual work reads:

$$\delta W = \int_\Omega \boldsymbol{C}\left(\varepsilon - \varepsilon_{eig}\right) : \delta\varepsilon \, d\Omega - \int_\Omega \boldsymbol{b}\delta\boldsymbol{u} - \int_{\Gamma_t} \boldsymbol{t}\delta\boldsymbol{u} = 0\,, \tag{2}$$

where **C** is the fourth-order stiffness tensor, $\boldsymbol{b}$ is the body force, and $\boldsymbol{t}$ is the traction force acting at the boundaries Γ_t. To represent the material heterogeneity, the Weibull distribution is chosen to obtain spread of material properties.

2.1 Aggregates modelling

In this model, aggregates are assumed to be composed of a quasi-brittle material. Each expanding ASR site creates compressive and tensile stresses in surrounding media. The tensile strength of aggregates and mortar is significantly lower than compressive counterpart. It suggests that locally material will always fail in tension. For this reason, we adopt the stress-based failure criterion. To compute damage, the crack band model originally proposed by Bazant [7] is chosen. The essence of

this model is to smear out existing micro-cracks over the fracture process zone of width w_c. The bilinear law adopted in this work is shown in Fig. 2.1. The area under the stress-strain curve equals the fracture energy G_c divided by the crack band width w_c:

$$\frac{G_c}{w_c} = \int_0^\infty \sigma d\varepsilon^f = \frac{1}{2} f_t^2 \left(\frac{1}{E} - \frac{1}{E_t}\right), \quad (3)$$

where ε^f is the fracturing strain. The ultimate strain ε_u becomes a function of the fracture energy, the crack band width, and the material strength in tension f_t:

$$\varepsilon_u = \frac{2G_c}{w_c f_t}. \quad (4)$$

Non-linear finite element method is widely used for modelling brittle materials with a single fracture path. However, it is often prone to numerical instabilities and divergence when there are multiple simultaneously growing cracks. The latter are widely present in the ASR-affected structures, and thus a different solution approach is required.

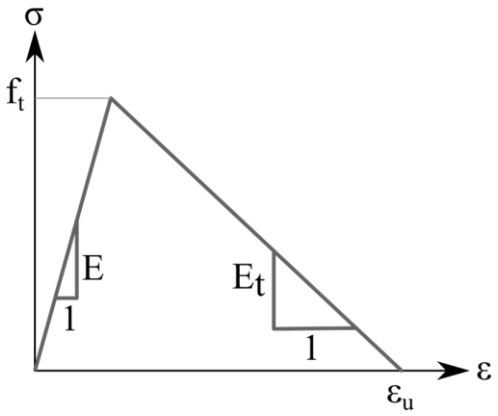

Figure 2.1. Bilinear law with the initial elastic loading phase and the linear strain-softening

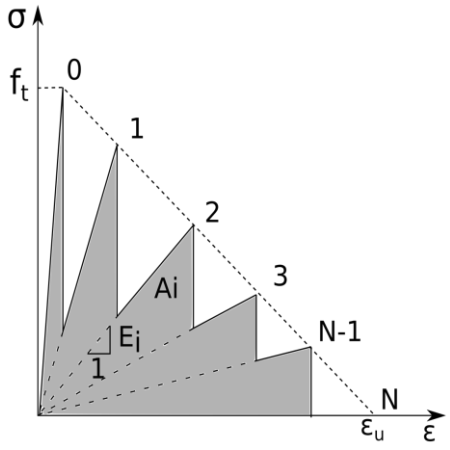

Figure 2.2. Saw-tooth diagram in the stress-strain space stemming from the sequential linear analysis

Sequential linear analysis (SLA) proposed by Rots and co-workers [8-9] facilitates solutions with extensive crack networks. This method was modified and applied to the ASR problem by Dunant and Scrivener [1] and CubaRamos et al. [2]. The basic idea of the latter is to replace a single loading step, where multiple elements are damaged, by several linear steps with a single broken element per step. The schematic of the SLA is shown in Fig. 2.2. After the stress σ in a single element reaches its strength f_t, the stiffness E_i and the tensile strength $f_{t,i}$ of this element is reduced according to the current damage value d_i which is defined by

$$d_i = 1 - \frac{1}{a^i}, \quad (5)$$

where *a*, the empirical reduction constant, is brought to the power *i,* which is the number of the reduction step. This is repeated until no more elements are damaged. Due to the discrete reduction of stiffness and strength, the stress-strain curve differs from the original softening one. Fig. 2.2 shows how in *N* iterations the stiffness of a single element is fully reduced to zero. Since the whole stress-strain path is followed by using only the secant stiffness, the tangent stiffness is not necessary, which reduces the possibility of numerical instabilities. However, the major drawback of this approach is its computational cost. Multiple integration points cannot be damaged simultaneously, which makes it necessary to re-compute the solution after each damage event. This computational load could, however, be optimized by allowing multiple elements to fail given that they are positioned at sufficient distance from each other.

2.2 Mortar modelling

In this study, we model mortar in elastic- and viscoelastic-brittle way and later compare the simulation results. The employed rheological model is the generalized Maxwell chain. It consists of a series of sequential spring-dashpots (Maxwell elements) placed in parallel with one single spring (see Fig. 2.3). The relation between stresses and strain comes from

$$\sigma(t) = \int_{-\infty}^{t} E(t,\tau)\boldsymbol{D}\dot{\varepsilon}d\tau\,, \tag{6}$$

where $E(t,\tau)$ is the time-dependent relaxation function, τ is the loading age, and $\boldsymbol{D}$ is the dimensionless matrix relating a 3D deformation state to a 1D relaxation function. The relaxation function is expanded in the exponential series

$$E(t,\tau) = E_0 + \sum_{\alpha=1}^{n} E_\alpha e^{-\frac{t-\tau}{\lambda_\alpha}}\,, \tag{7}$$

where the relaxation time of each Maxwell element is defined as $\lambda_\alpha=\eta_\alpha/E_\alpha$ with η_α being the viscosity of a dash-pot. Assuming a constant strain rate within each time step, the analytical integration of the right-hand side of Eq. 7 leads to the following form

$$\sigma(t+\Delta t) = E_0\boldsymbol{D}\varepsilon + \sum_{\alpha=1}^{n}\left(\left(1-e^{-\frac{\Delta t}{\lambda_\alpha}}\right)\frac{E_\alpha\lambda_\alpha}{\Delta t}\boldsymbol{D}\Delta\varepsilon + e^{-\frac{\Delta t}{\lambda_\alpha}}\sigma_\alpha(t)\right), \tag{8}$$

with $\sigma_\alpha(t)$ being the internal stress within each Maxwell element, defined as

$$\sigma_\alpha(t) = \boldsymbol{D}\int_{\boldsymbol{0}}^{\boldsymbol{t}} E_\alpha e^{-\frac{t-\tau}{\lambda_\alpha}}\dot{\varepsilon}d\tau\,, \tag{9}$$

The first term under the sum sign in Eq. 8 could be seen as the effective stiffness of a single Maxwell element multiplied by the matrix $\boldsymbol{D}$ and the strain increment $\Delta\varepsilon$:

$$E_\alpha^{ef} = \left(1-e^{-\frac{\Delta t}{\lambda_\alpha}}\right)\frac{E_\alpha\lambda_\alpha}{\Delta t}, \tag{10}$$

Time increment Δt controls the rate dependency of the effective stiffness. By limit analysis, we find the limiting values of the effective stiffness which are equal to E_0 for infinitely slow loading (Δt tending to 0) and $E_0+\Sigma E_\alpha$ for infinitely fast (Δt tending to infinity). At the end of each converged time step, the internal stress $\sigma_\alpha(t)$ is updated according to

$$\sigma_\alpha(t) = \sigma_\alpha(t-\Delta t)e^{-\frac{\Delta t}{\lambda_\alpha}} + E_\alpha^{ef}\boldsymbol{D}\Delta\varepsilon\,, \tag{11}$$

In this study, the damage is affecting viscoelastic material by reducing both the stiffnesses of the spring elements E_i and the viscosities of the dash-pots η_i by the factor $(1-d)$. The influence of temperature on viscoelasticity is neglected.

Relaxation times of the mortar were calibrated by the creep experiments on 28 day-old concrete by L'Hermite [10]. In this test, a block of concrete was loaded with 9.81 MPa. Model calibration was done on a 2D concrete block with purely elastic aggregates and viscoelastic mortar. Both experimental and numerical strain values along the deformed axis are reported in Fig. 2.4. There is a fair agreement between two sets of values. The viscoelastic properties of the mortar are given in Tab.2.1.

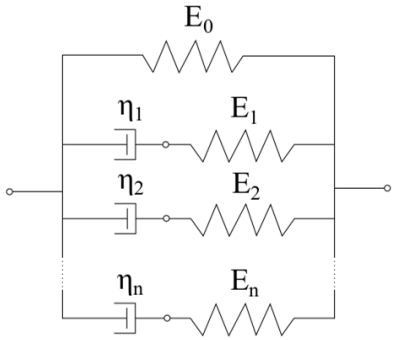

Figure 2.3. Generalized Maxwell chain

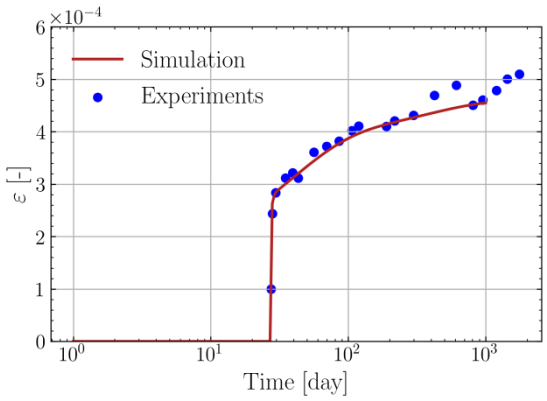

Figure 2.4. Deformation of a 2D concrete model compared with the experimental values by L'Hermite [10]

Table 2.1: Properties of the concrete components

Property	Aggregates	Mortar (elastic-brittle)	Mortar (viscoelastic-brittle)	ASR product
Single spring stiffness E_0, GPa	60	19	6	11
Maxwell stiffness E_i & relaxation time λ_i, GPa/days	-	-	5 / 0.5 6.5 / 20 1.5 / 67	-
Poisson ratio v, -	0.3	0.3	0.3	0.18
Tensile strength f_t, MPa	10	4	4	-
Fracture energy G_c, Jm^{-2}	160	80	80	-
Latency time τ_{lat}, days	-	-	-	10
Characteristic time τ_{ch}, days	-	-	-	110
Asymptotic strain $\varepsilon(\infty)$, -	-	-	-	0.115

A combination of the viscoelasticity with sequential linear analysis is not a trivial task, and to the best of these authors' knowledge was not previously reported in the literature. The major challenge in its implementation is the rate-dependency of stress and thus a non-unique path in the stress-strain space. However, if we assume that the fracture energy does not change with the loading rate and the initial elastic stiffness is much higher than the softening slope, then the slope of the softening branch will be similar to the elastic one. When the softening slope is fixed, generalized Maxwell chain behaves elastically with linear softening in two limiting cases: when the loading rate is either infinitely high or infinitely low (see Fig. 2.5). Intermediate loading rates will result in a stress-strain curve

positioned in-between the limiting ones. This property was used to develop equations for the viscoelastic strain-softening law. The ultimate strain ε_u will now depend on the loading rate through the effective stiffness E_α:

$$\varepsilon_u = \frac{2G_c}{w_c f_t} - \frac{f_t}{E_0 + \sum E_\alpha} + \frac{f_t}{E_0 + \sum E_\alpha^{ef}} \,. \tag{12}$$

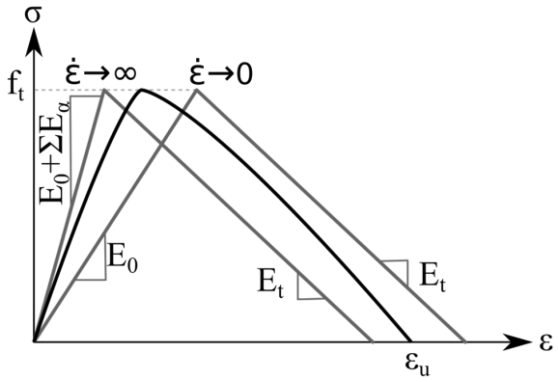

Figure 2.5: Constitutive law combining viscoelasticity with damage. Two different loading rates result in different values of softening strain. The softening slope is preserved.

In this way, the decrease in the loading rate will result in an increase in ε_u with the slope E_t remaining unchanged.

Procedures of SLA are adapted to include viscoelasticity as follows (see Fig. 2.6):

1. The loading is applied and finite element problem is solved. Existing damage is accounted in the reduced values of stiffness and viscosity. Internal stresses are updated.
2. The strength criterion in the element with the highest stress is verified. In case of its violation, the damage parameter *d* is increased. The strength, stiffness, and viscosity of the damaged element are reduced accordingly.
3. The displacement field is reset.
4. Steps 1-3 are repeated until no damaging events are present.
5. The next loading step is done. Time step Δt within the viscoelastic material is set to the time of the current step.

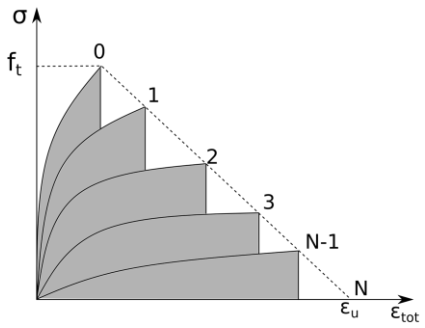

6.

Figure 2.6: Viscoelastic extension of SLA. Every loading step is viscoelastic, starting at zero displacements.

Since every solution in time is obtained via a direct jump from zero displacements to the current loading, the time correction is necessary to scale properly the viscoelastic effect. The solution obtained in such manner will differ from the one obtained incrementally (using information from previous steps). The reason is that the proposed scheme does not take into consideration loading history between the zero and the current step: loading is assumed to increase linearly. This approximate way of solving a viscoelastic problem will introduce a certain error. However, we argue that for relatively short relaxation times λ this difference will be less pronounced. This is demonstrated in Fig. 2.6. A single finite element of the viscoelastic-brittle mortar with properties given in Tab. 1 is deformed by strain ε. In this simulation, the element does not experience any damage. Sequential and

incremental stress values differ from each other by 5-10%. In case of the S-shaped loading profile (left figure), sequentially computed stress slightly exceeds the incremental one. In the later stage, it steadily tends toward the incremental curve due to stronger stress relaxation. This loading profile is of primary importance since it is similar to the one we will use for the ASR product expansion, which will be discussed in the following sub-section. A sinusoidal profile shown in the right figure is brought to demonstrate that harmonic load fluctuations do not lead to the error augmentation either.

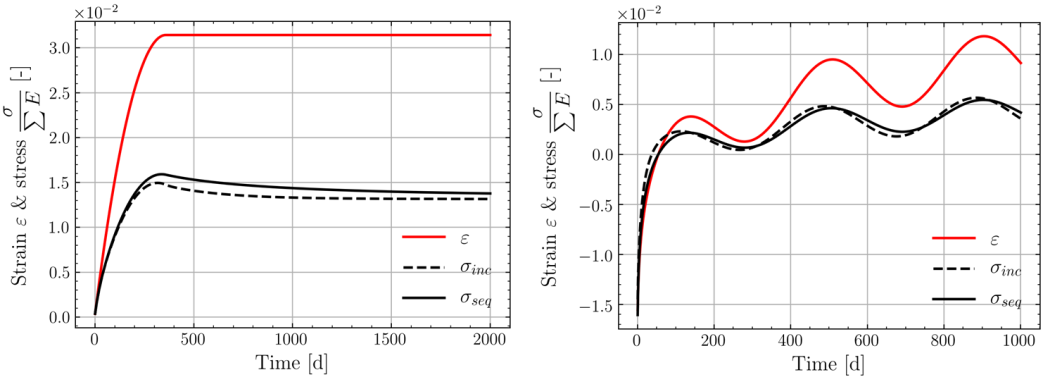

Figure 2.7: Comparison of stresses in a viscoelastic material computed in incremental and sequential manners. The S-shaped loading is shown in the left figure and the sinusoidal one in the right.

2.3 ASR product expansion

Dependence of alkali-silica reaction kinetics on the temperature and the relative humidity was experimentally studied by Larive [11]. First-order kinetic law in isothermal conditions results in explicit equation for the chemical extent ξ:

$$\xi(t,T) = \frac{1 - e^{-\frac{t}{\tau_{ch}(T)}}}{1 + e^{-\frac{t}{\tau_{ch}(T)} + \frac{\tau_{lat}(T)}{\tau_{ch}(T)}}}, \tag{13}$$

where t and T are the current time and temperature, and τ_{lat} and τ_{ch} are latency and characteristic times correspondingly. The latter two are calibration parameters of the model.

In this study, we assume that the local strain of an ASR site ε_{eig} is proportional to the total amount of the generated ASR product which in its turn is proportional to the chemical extent ξ. This way, the ASR expansion law reads:

$$\varepsilon(t,T) = \varepsilon(\infty)\frac{1 - e^{-\frac{t}{\tau_{ch}(T)}}}{1 + e^{-\frac{t}{\tau_{ch}(T)} + \frac{\tau_{lat}(T)}{\tau_{ch}(T)}}}, \tag{14}$$

where ε(∞) is the asymptotic strain. If the temperature of a specimen is homogeneous, all the ASR sites will have same expansion values.

3. SIMULATIONS

In order to study the effect of viscoelasticity we have simulated ASR deterioration of a concrete specimen in laboratory conditions. For this, we use a two dimensional model of size 72 by 72 mm (see Fig. 2.8 left). The simulated concrete block consists of circular aggregates with packing density of 70%, mortar, and ASR sites. Free expansion boundary conditions are applied in a form of 3 corner nodes fixed in either two directions (left bottom node) or one direction (left top and right bottom nodes). Other surface nodes are free to move. Material and thermal law (Eq. 14) parameters are given in Tab. 1. Stiffness of the elastic-brittle mortar is chosen to be equal to the sum of spring stiffnesses in the Maxwell chain of the viscoelastic-brittle mortar. This way, the elastic material behaves as if it would be a viscoelastic one under infinitely fast loading. Such a choice of material properties facilitates a fair comparison of two simulations. The parameters of the thermal law were calibrated with experimental data on accelerated free ASR expansion of concrete blocks during 450 days by Multon and Toutlemonde [12].

Concrete undergoing free ASR expansion was simulated for 450 days at the temperature of 38°C. The damage pattern obtained within concrete blocks in case of the elastic- and viscoelastic-brittle mortar is shown in Fig. 2.8 (center, right). In both cases, the damage is mainly spread within mortar due to its lower tensile strength. One could also observe that in case of the elastic-brittle mortar there is larger damaged area than in the viscoelastic-brittle case. This becomes evident in Fig. 2.9 (right) where the damage ratio is plotted. It is the ratio between the damaged area of a phase and its total area. To compute this parameter, the area of each damaged element from a specific phase is multiplied by its damage value *d*, summed together and divided by the total area of this phase. Damage in the elastic-brittle mortar is 5% higher than in its viscoelastic counterpart. Reduction in the damage ratio is mainly caused by the lower values of stress within viscoelastic material due to the stress relaxation. The damage ratio within aggregates saturates at the value of 2% already at 120 days. This effect is caused by having all the cracks reaching exteriors of aggregates, after which no additional damage to aggregates is caused. For the mortar, saturation happens much later and has a higher value.

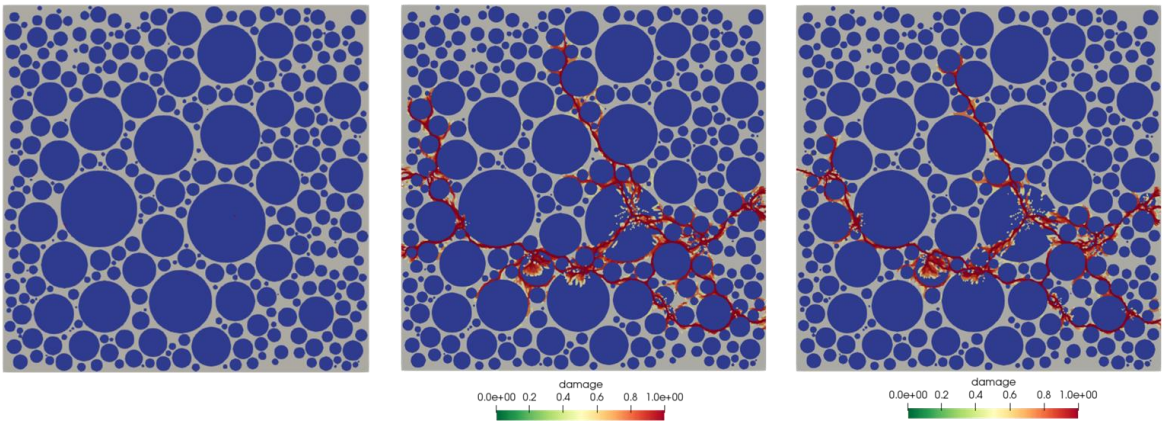

Figure 2.8. A 2D concrete specimen (left) comprising three phases: aggregates (blue), mortar (grey) and 10 ASR sites (not visible due to their size). Damage patterns in concrete blocks with the elastic (centre) and viscoelastic (right) mortar. Colours denote the level of damage.

Fig. 2.9 (left) shows the macroscopic expansion of the specimen in horizontal and vertical directions, the experimental data [12] used for the model calibration as well as the ASR product expansion curve. In this specific distribution of ASR sites, major crack percolate in the horizontal direction (see Fig. 2.8). It has wide opening in the vertical direction forcing the corresponding macroscopic strain ε_y *to* be larger than the horizontal one ε_x. Although these two curves differ significantly, their mean value is close to the calibration curves. The expansion of the viscoelastic-brittle mortar in the same figure is similar in the vertical direction but much lower in horizontal. This fact is again caused by shorter cracks in the viscoelastic paste and thus lower expansion. The average between horizontal and vertical values becomes lower than the calibration data. The S-shaped expansion curves follow a similar trend in the ASR product expansion ε_{eig}.

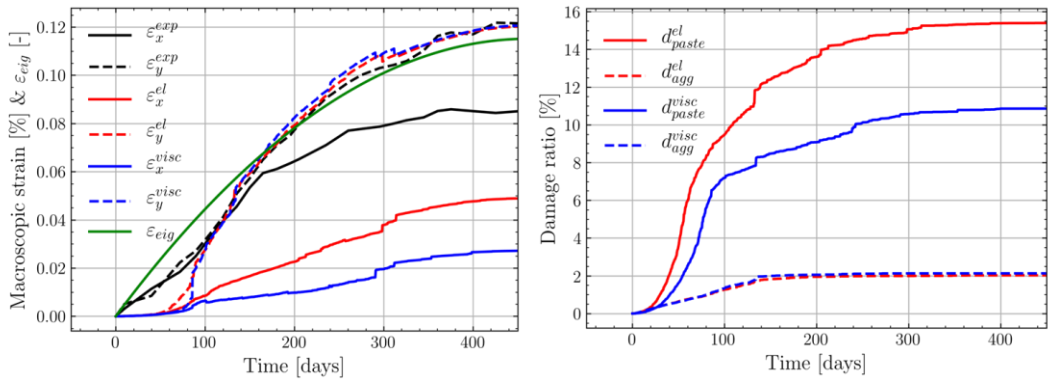

Figure 2.9: The macroscopic expansion of the concrete specimen (left) and its damage ratio (right)

Stiffness reduction in two directions is plotted in Fig. 2.10 (left). Here we also observe approximately total stiffness loss in the vertical direction due to the percolated crack. In the other direction, stiffness drops to 40-50% of its initial value due to vertical cracks yet not reaching the specimen boundaries. Stiffness reduction in the horizontal direction is lower in the elastic-brittle case. This is also explained by the elastic-brittle mortar having longer cracks in vertical and close to vertical directions the viscoelastic one.

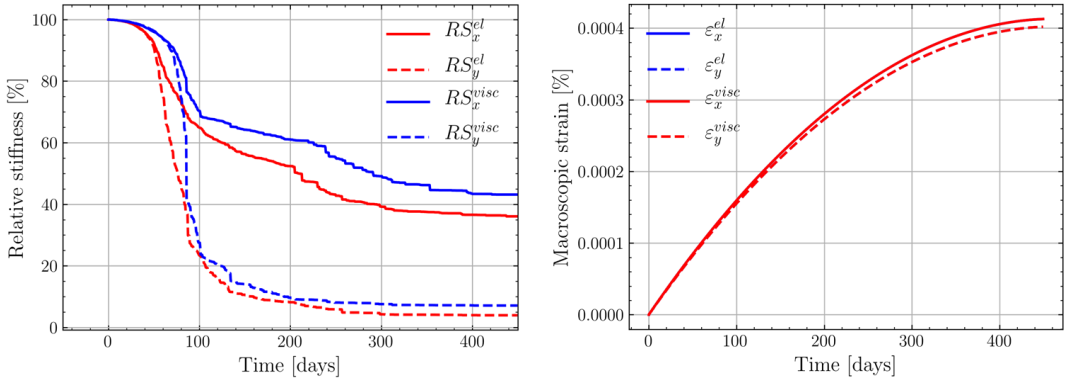

Figure 2.10. Left) stiffness reduction for elastic- and viscoelastic-brittle cases. Right) Macroscopic expansion for purely elastic and viscoelastic cases without damage.

When adding viscoelasticity to the mortar, we indeed observe a lower stiffness drop as it was suggested by Cuba Ramos and co-workers [8]. This however results also in the reduction of the macroscopic strain due to the shortening of cracks. The reduced strains are lower than the ones observed by the experimentalists. We suggest that the total damage observed in the concrete (either in mortar or in aggregates) is insufficient to reach the experimental values of expansion. To prove that the damage is the main cause of the macroscopic expansion, we run two simulations where the mortar is modeled either purely elastic or viscoelastic and no damage is happening. The results are plotted in Fig. 2.10 (right). Expansion in each direction is equal for both simulations because of ASR eigenstrain being an internal boundary condition. The final value of expansion is however three orders of magnitude lower than in the brittle case. This demonstrates that purely (visco-) elastic deformation is not sufficient to bring the macroscopic expansion to the experimental levels, and cracks are necessary.

Giorla et al. [4] also reported little damage in the viscoelastic mortar which corresponded to the general observations in experiments. However, the macroscopic expansion was lower than the experimental values of Ben Haha [13]. As a cause, the authors suggested the fact that the smaller aggregates were not reactive in their simulations. We also think adding more ASR sites to aggregates in our model would result in higher macroscopic expansion without significantly increasing crack extent in the mortar.

4. CONCLUSIONS

In this paper, a numerical model to solve material deterioration due to multiple crack growing has been presented. Extension of the elastic-brittle material behavior to viscoelasticity has been formulated and demonstrated on an example. Laboratory concrete specimens undergoing damage due to alkali-silica reaction were simulated. In order to understand the role of viscoelasticity in the ASR damaging process, the simulation with the elastic-brittle mortar was compared to the viscoelastic-brittle one. The simulation results can be summarized as follows:

- The macroscopic expansion of specimens is mainly caused by crack growth and opening. Direction of expansion is orthogonal to the crack path.
- Most of the damage is concentrated inside the mortar due to its lower tensile strength.
- The macroscopic strain curve follows the trend of the ASR product expansion curve.
- Viscoelastic-brittle behavior of the mortar causes relaxation of stresses and thus reduction of damage. It leads to the preservation of the macroscopic stiffness but also reduces the macroscopic expansion of concrete.

- For the macroscopic expansion to reach the experimental levels without significantly affecting the amount of cracks in the paste, more damage should happen in the aggregates only.

5. ACKNOWLEDGMENTS

The financial support of the Swiss National Science Foundation within the Sinergia-project “Alkali-silica reaction in concrete (ASR)”, grant number CRSII5_171018.

6. REFERENCES

[1] Dunant CF, Scrivener KL (2010) Micro-mechanical modelling of alkali–silica-reaction-induced degradation using the amie framework. Cement and Concrete research 40(4):517–525.

[2] Cuba Ramos AI, Roux-Langlois C, Dunant CF, Corrado M, and Molinari J-F (2018) HPC simulations of alkali-silica reaction-induced damage: Influence of alkali-silica gel properties. Cem. Concr. Res., 109(April):90–102. ISSN 00088846. doi: 10.1016/j.cemconres.2018.03.020.

[3] Beushausen H, Chilwesa M (2013) Assessment and prediction of drying shrinkage cracking in bonded mortar overlays. Cem. Concr. Res., 53:256–266.

[4] Giorla AB, Scrivener KL, Dunant CF (2014) Influence of visco-elasticity on the stress development induced by alkali-silica reaction. Cem. Concr. Res., 70:1–8, 2015. ISSN 00088846. doi: 10.1016/j.cemconres.2014.09.006.

[5] Leemann A, Münch B (2019) The addition of caesium to concrete with alkali-silica reaction: Implications on product identification and recognition of the reaction sequence. Cem. Concr. Res., 120:27–35. ISSN 0008-8846. doi: 10.1016/J.CEMCONRES.2019.03.016.

[6] Leemann A, Katayama T, Fernandes I, and Broekmans MATM (2016) Types of alkaliaggregate reactions and the products formed. Proc. Inst. Civ. Eng. - Constr. Mater., 169(3):128–135. ISSN 1747-650X. doi: 10.1680/jcoma.15.00059

[7] Bažant ZP, Oh BH (1983) Crack band theory for fracture of concrete. Mat. Constr. 16, 155–177. https://doi.org/10.1007/BF02486267

[8] Rots JG (2001) Sequentially linear continuum model for concrete fracture. Fract. Mech. Concr. Struct. Proc. 4th Int. Conf. Fract. Mech. Concr. Concr. Struct., pages 831–839. ISSN 00223050. doi: 10.1136/jnnp-2014-307772.

[9] Rots JG, Invernizzi S (2004) Regularized sequentially linear saw-tooth softening model. International Journal for Numerical and Analytical Methods in Geomechanics 28(7-8):821–856.

[10] L'Hermite RG (1965) Nouveaux resultants de recherches sur la deformation et la rupture du beton. Annales de 1'Institut Technique du Batiment et des Travaux Publics 18(207):325-59.

[11] Larive C (1998) Apports combinés de l’expérimentation et de la modélisation à la compréhension de l’alcali-réaction et de ses effets mécaniques. PhD thesis, Laboratoire Central des Ponts et Chaussées, Paris, France.

[12] Multon S, Toutlemonde F (2006) Effect of applied stresses on alkali-silica reaction-induced expansions. Cem. Concr. Res., 36(5):912–920.

[13] Ben Haha M, Gallucci E, Guidoum A, Scrivener KL (2007) Relation of expansion due to alkali silica reaction to the degree of reaction measured by SEM image analysis. Cem. Concr. Res., 37(8):1206–1214. ISSN 00088846. doi: 10.1016/j.cemconres.2007.04.016.